Chaos and Anderson-like localization in polydisperse granular chains

V. Achilleos,[1] G. Theocharis,[1] and Ch. Skokos[2]
[1]*Laboratoire d'Acoustique de l'Université du Maine, UMR CNRS 6613 Av. O. Messiaen, F-72085 LE MANS Cedex 9, France*
[2]*Department of Mathematics and Applied Mathematics, University of Cape Town, Rondebosch 7701, South Africa*

(Received 2 July 2017; revised manuscript received 20 October 2017; published 27 April 2018)

We investigate the dynamics of highly polydisperse finite granular chains. From the spatiospectral properties of small vibrations, we identify which particular single-particle displacements lead to energy localization. Then, we address a fundamental question: Do granular nonlinearities and the resulting chaotic dynamics destroy this energy localization? Our numerical simulations show that for moderate nonlinearities, the overall system behaves chaotically, and spreading of energy occurs. However, long-lasting chaotic energy localization is observed for particular single-particle excitations in the presence of the nonsmooth nonlinearities. On the other hand, for sufficiently strong nonlinearities, the granular chain reaches energy equipartition. In this case, an equilibrium chaotic state is reached independent of the initial position excitation.

DOI: 10.1103/PhysRevE.97.042220

I. INTRODUCTION

Granular solids are densely packed assemblies of polydisperse grains commonly found in nature and industry [1–3]. Recent technical and conceptual advances on the vibrational analysis of micro [4–6] and macro [7] granular solids led to a better understanding of their dynamics and revealed novel mechanical features. In addition, mesoglasses made as granular assemblies of brazed aluminum beads have also been used for fundamental studies in glass physics, including classical (elastic) Anderson localization [8] and its mobility gaps [9]. However, to further probe the intrinsic transport and mechanical properties of granular solids, a deeper understanding of the *anharmonic* grain contact interactions is required [3]. These, in combination with features such as structural disorder and polydispersity, make the vibrational energy transport in granular solids a complex, open major challenge in physics. To this end, studies of the simplified system of polydisperse granular *chains* are essential for a better understanding of energy transport in granular solids.

Granular chains are a vibrant and rapidly expanding area of research [10–14], providing a test bed for fundamental studies of nonlinear dynamics including solitary waves, breathers, nonlinear normal modes, as well as different engineering applications such as tunable waveguides, shock- and energy-absorbing layers, and acoustic diodes. Regarding polydisperse chains, several studies [12,15–17] have been devoted to the highly nonlinear regime where precompression forces are absent and the structure acts as a sonic vacuum that does not transmit sound. Recently, few studies on the dynamics of disordered granular chains in the presence of precompression forces have also appeared [18–20] showing that energy transfer varies significantly from the strongly precompressed (near linear) limit to the weakly compressed (highly nonlinear) regime. This is due to the unique nature of the system, allowing the coexistence of extended and localized modes, along with the particular granular nonlinearities featuring a smooth nonlinearity due to Hertzian contact interactions and a nonsmooth nonlinearity (contact breakings) at the same time. These features make granular chains fundamentally different from other nonlinear lattices [such as the discrete Klein-Gordon (KG) and the discrete nonlinear Schrödinger (DNLS) systems].

Aiming for a better understanding of energy localization and transport in polydisperse granular solids, we investigate in this work the dynamics of a strongly polydisperse granular chain under single-particle displacements. Polydispersity induces strong energy localization (Anderson-like localization) in the system in the linear regime. Here we investigate the fate of the Anderson-like localization in the presence of granular nonlinearities by numerically investigating single-particle displacement excitations. In particular, we study the time evolution of such excitations starting from the system's linear limit, continuing to its weakly nonlinear regime, where we observe localized chaotic behaviors, and finally moving to the model's highly nonlinear regime where energy delocalization and equipartition occurs.

Note that Anderson localization in other nonlinear lattices such as the KG and DNLS systems has been extensively studied [21–25]. For the aforementioned systems, it is now established that whether nonlinear Anderson localization persists or is destroyed (leading to energy spreading) is associated with chaos and has probabilistic features [26]. Our results reveal a much richer dynamical response, including chaotic energy spreading, long-lived chaotic Anderson-like localization, and energy equipartition. In particular, we find that although the overall system behaves chaotically in the weakly nonlinear regime, it can exhibit long-lasting energy localization for particular single-particle excitations.

The paper is organized as follows: in Sec. II, after introducing the model, we present a normal mode analysis and we highlight how single-site excitations lead to Anderson-like localization in the linear regime. In Sec. III, by performing long-time simulations in the weakly nonlinear regime, we present the fate of different initially localized excitations, studying in detail the energy spreading or its absence and their chaotic dynamics. Then, in Sec. IV we study the strongly nonlinear regime where

an equilibrium chaotic state is reached independent of the initial position excitation. Finally, in Sec. V we summarize our results and present the conclusions of our study.

II. MODEL, NORMAL MODES, AND LOCALIZATION

The structure studied in this work consists of a chain of N spherical particles in contact, having masses m_n ($n = 1,2,\ldots,N$). The corresponding Hamiltonian H (whose value represents the system's energy) is given by

$$H = \sum_{n=1}^{N} H_n \equiv \sum_{n=1}^{N} \left(\frac{p_n^2}{2m_n} + V_n \right), \tag{1}$$

where H_n and $p_n = m_n \dot{u}_n$ are the energy and momentum of the nth spherical particle, respectively, with u_n being the displacement of this particle from its equilibrium position, while an overdot denotes differentiation with respect to time. The potential V_n for each particle is defined as $V_n = [V(u_n) + V(u_{n+1})]/2$, where

$$V(u_n) = \tfrac{2}{5} A_n [\delta_n + u_{n-1} - u_n]_+^{5/2} - \tfrac{2}{5} A_n \delta_n^{5/2} - A_n \delta_n^{3/2} (u_{n-1} - u_n). \tag{2}$$

In Eq. (1), hard wall boundary conditions, $u_0 = u_{N+1} = 0$, are used. In Eq. (2), δ_n is the relative static overlap due to a precompression force F acting on the chain and is given by $\delta_n = (F/A_n)^{2/3}$ [27], where A_n is the contact coefficient between particles $n-1, n$. For spheres of the same material, $A_n = (2/3)\mathcal{E}\sqrt{(R_{n-1}R_n)/(R_{n-1}+R_n)}/(1-\nu^2)$ [27], with $\mathcal{E}$, ν, and R_n being the elastic modulus, Poisson's ratio, and the radius of the n bead, respectively. In our simulations, we choose units corresponding to a mean radius of $R = 0.01$ m and a static force $F = 1$ N. The elastic modulus is chosen as $E = 193$ GPa and the Poisson ratio is $\nu = 0.3$ relevant to stainless steel (316 type). The terms $[\ ]_+$ in Eq. (2) vanish when their argument becomes negative. This happens when a *gap* between two particles appears, i.e., $u_{n-1} - u_n > \delta_n$. Note that the second (constant) term of the potential in Eq. (2) is added in order to have a zero total energy when all particles are in their equilibrium position, i.e., $u_n = 0$ for all n. The last term of the potential, which is linear in u_n, does not contribute to the total energy since all terms cancel out.

We normalize the system by using as a reference the uniform chain with particles of radius $\tilde{R} = (\alpha+1)R/2$, where $\alpha = \max(R_n)/\min(R_n)$ is the disorder strength. Then time, distance, mass, and stiffness are scaled as follows: $t \to \tilde{\omega} t$, $\delta_n \to \delta_n/\tilde{\delta}$ ($u_n \to u_n/\tilde{u}$), $m_n \to m_n/\tilde{m}$, and $A_n \to A_n/(6\tilde{A})$, where all the quantities with a tilde are calculated at $\tilde{R}$. Normalization is such that in the case of no disorder ($\alpha = 1$), the normalized linear cutoff frequency is $\omega = 1$. The model composed by Eqs.(1) and (2) has been extensively studied in the context of granular chains [10–14]. Considering sufficiently small displacements, $u_n \ll 1$, we obtain a linearized Hamiltonian with potential $V(u_n) = K_n(u_{n-1} - u_n)^2/2$, where $K_n = (4/3)A_n\delta_n^{1/2}$ [27] is the linear coupling constant.

Aiming at an understanding of energy localization in strongly polydisperse granular chains, we generate a disorder setup of $N = 100$ spheres whose radii R_n are taken from a uniform distribution, within the range $R_n \in [R, \alpha R]$ with $\alpha = 5$.

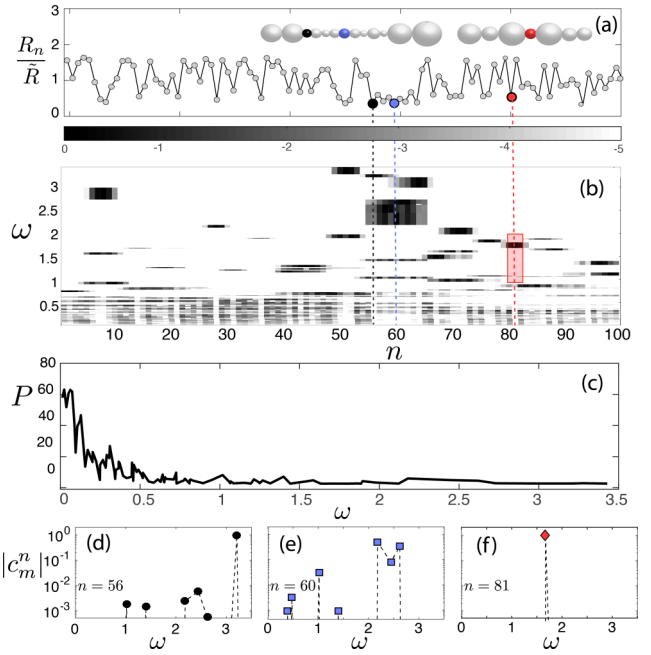

FIG. 1. (a) The random distribution of the normalized radii considered here. Insets show the spheres in scale, in the neighborhood of $n = 60$ and 81. (b) Contour plot of the coefficients $\log|c_m^n|$, obtained when projecting an initial displacement of particle n onto the normal modes of frequency ω. The color bar on the top of panel (b) is in logarithmic scale. (c) The participation number P of the eigenmodes as a function of their frequency. (d)–(f) The largest coefficients $|c_m^n|$ for the initial displacement of particles $n = 56$, 60, and 81, respectively, in logarithmic scale.

The considered distribution of normalized radii is shown in [Fig. 1(a)]. Then, for the rest of the work, we keep this particular configuration and we investigate the long-time dynamics under different single-particle displacement excitations.

First, we obtain the harmonic eigenmodes and we calculate their participation number given by the expression $P = 1/\sum h_n^2$, where $h_n = H_n/H$ [Fig. 1(c)]. At low frequencies, there are around 10 modes with $P > 40$, namely modes that exhibit a localization length of the order of the length of the chain. These modes, called also propagons [28], are responsible for the transport of energy [29] of the linearized granular chain, which is an FPU-like lattice. The remaining modes, called also locons [28], are localized. As an additional note, we comment that due to the strong polydispersity, there are at least 20 highly localized modes with $P \lesssim 3$.

In Fig. 1(b) we plot the projection coefficients c_m^n of all the possible single-site displacement excitations (of the form $\vec{u}^{\,n}(0) = [0,0,\ldots,1,\ldots,0]$) onto the normal modes of the harmonic chain. The index n [x axis of Fig. 1(b)] counts the number of particles that are displaced and m counts the number of normal modes when they are ordered with increasing frequency ω [y axis of Fig. 1(b)]. In Figs. 1(d)–1(f) we show the projection coefficients (with $|c_m^n| > 10^{-4}$) of three cases onto the normal modes.

From Fig. 1(b), one is able to identify particular single-particle displacement excitations whose projection coefficients at the low-frequency regime (where the extended modes are

located) are highly suppressed. This is monitored by the existence of white areas at the low-frequency regime ($\omega < 0.2$). As a consequence, these single-site excitations provoke Anderson localization, and the initial energy input into the system remains localized.

Three examples of single-site excitation leading to localization are $n = 56$, 60, and 81, whose coefficients $|c_m^n|$ are shown in Figs. 1(d)–1(f). The case of $n = 56$ in Fig. 1(d) contains the strong excitation of one mode at frequency $\omega \approx 3.189$ and additional other weakly excited modes. The case of $n = 60$, as shown in Fig. 1(e), corresponds to a multiple mode excitation while the case of 81, as shown in Fig. 1(f), corresponds to an almost single-mode excitation. Below, we choose to investigate in detail these three particular cases since they summarize the different long-time dynamics of an initially localized energy in the presence of weak nonlinearities. Other choices of initial single-site excitations bearing similar coefficients to those in Figs. 1(d)–1(f) exhibit the same behavior.

III. FATE OF LOCALIZATION: WEAKLY NONLINEAR REGIME

The natural question that arises is how the granular nonlinearities influence the aforementioned localization. Should we also expect a chaos-induced destruction of localization and diffusive energy spreading, as is the case of KG and DNLS lattices? To answer these fundamental questions, we investigate the long-time dynamics of the chain. In particular, we perform simulations up to $t = 10^7$ normalized time units using a symplectic integration scheme [30] after initially displacing particles $n = 51$, 60, and 81.

We start by studying the case of moderate nonlinearities by imposing initial displacements corresponding to a small amount of energy. As we show below, the long-time dynamics of these three initial excitations, for sufficiently weak nonlinearities, exhibit different chaotic behaviors as well as different energy-spreading mechanisms.

In particular, for particle $n = 56$, we use an initial energy $H = 0.049$, while for particles $n = 60$ and 81 we use $H = 0.192$. The corresponding spatiotemporal evolution of the energy for the three cases is shown in Fig. 2, where the color map is in a logarithmic scale. The energy spreading is monitored by calculating the participation number P and the second energy moment $m_2 = \sum_n (n - \tilde{n})^2 H_n$, where $\tilde{n} = \sum n H_n$. The system's chaoticity is quantified using the maximum Lyapunov characteristic exponent (mLCE) λ [31,32], which is obtained by numerically integrating both the Hamilton equations of motion and the corresponding variational equations [33]. The variational equations govern, at first order of approximation, the time evolution of a deviation vector $\vec{w}(t) = [\delta u_1, \delta u_2, \ldots, \delta u_n, \delta p_1, \delta p_2, \ldots, \delta p_n]$, where δu_i, δp_i, $i = 1, 2, \ldots, N$, are, respectively, small perturbations from the studied orbit in positions and momenta (see [32] and references therein). Note that λ is evaluated as $\lambda = \lim_{t\to\infty} \Lambda(t)$, where $\Lambda(t)$ is the so-called finite-time mLCE [32]. For chaotic orbits, $\Lambda(t)$ eventually converges to a positive value, while for regular orbits it tends to zero following the power law $\Lambda(t) \propto t^{-1}$ [32].

As is directly seen from Fig. 2, there are differences in the long-time energy distribution between the three initial excitations. In addition, from Fig. 2(d) one can also clearly see that in all cases, $\Lambda(t)$ eventually diverges from the law proportional to t^{-1} (denoted by the dashed line) and thus the system exhibits chaos.

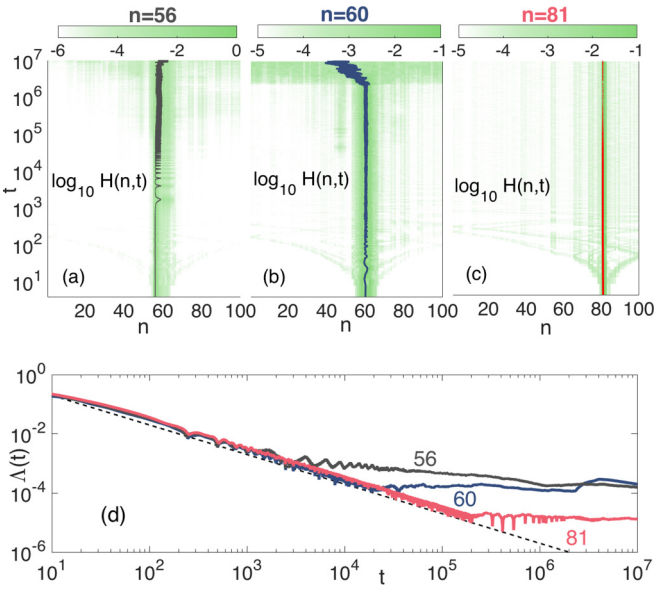

FIG. 2. (a)–(c) The spatiotemporal evolution of energy after exciting particle $n = 56$ (a) with energy $H = 0.049$ and particles $n = 60$ (b) and $n = 81$ (c) with energies $H = 0.192$. Color bars on top of the panels are in logarithmic scale. The solid curves show the mean position of the energy distribution. (d) The finite-time mLCE $\Lambda(t)$ as a function of time for the three different cases of panels (a)–(c). The dashed line denotes the law $\Lambda(t) \propto t^{-1}$ appearing for the case of regular motion.

A. Energy spreading and weak chaos

We first study in detail the dynamics resulting from the excitation of particle 56 shown in Fig. 2(a). As is observed, the energy remains almost localized around particle 56, at least up to $t \approx 10^5$, and then energy appears to be spreading to more particles. The mean energy position, shown with the solid line, exhibits characteristic oscillations. These oscillations are more evident in the evolution of m_2 and on the participation number P shown in Fig. 3. From this figure we see that although the energy remains localized, initially it is exchanged between

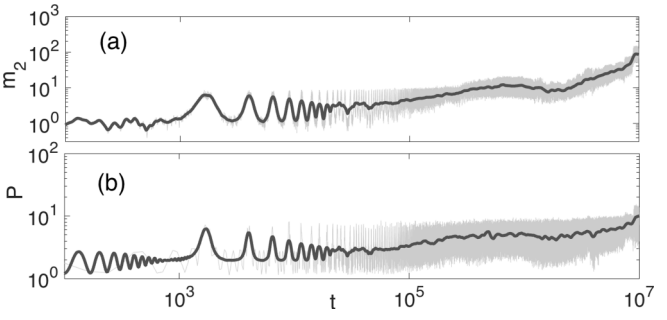

FIG. 3. Time evolution of the second energy moment m_2 (a) and the participation number P (b) after the initial displacement of particle $n = 56$ with energy $H = 0.049$. The solid curves correspond to the running averages of the plotted quantities.

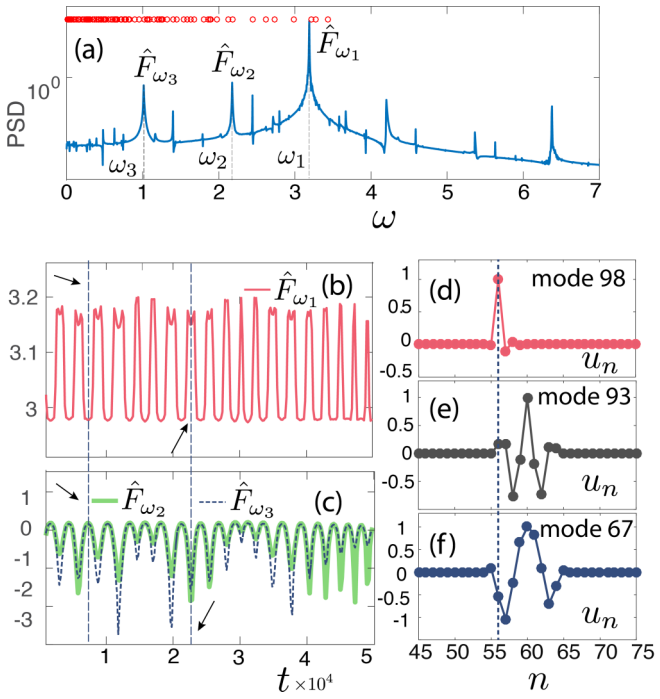

FIG. 4. (a) The power spectral density (PSD) of the velocity of particle $n = 56$. The circles in the top of the panel indicate the eigenfrequencies of the linear system, while the frequencies corresponding to the three highest peaks of the PSD are denoted as ω_1, ω_2, and ω_3. (b) The time evolution of the logarithm of the amplitude $\hat{F}_{\omega_1}$ of the PSD (a) at frequency ω_1. (c) The same as (b) but for the amplitudes $\hat{F}_{\omega_2}$ (solid curve) and $\hat{F}_{\omega_3}$ (dashed curve) of frequencies ω_2 and ω_3 of (a). (d)–(f) The three linear eigenvectors with frequencies close to the shifted frequencies ω_1, ω_2, and ω_3 of (a). The vertical dashed line denotes the position of particle $n = 56$.

two to eight particles. At $t \approx 10^4$, m_2 starts increasing with a small slope, suggesting a slow spreading, while after $t \approx 10^6$ it tends to increase with an even larger slope signaling a faster spreading also evident in the energy profile in Fig. 2(a). As the energy spreads, more particles (degrees of freedom) are excited and the total amount of energy is distributed to more and more particles.

Accordingly, the finite-time mLCE $\Lambda(t)$ for this excitation shown in Fig. 2(d) is found to deviate from the law $\Lambda(t) \propto t^{-1}$ appearing for the case of regular motion and thus the dynamics is chaotic. However, since most of the degrees of freedom are initially "mute" and start to contribute to the dynamics only when the energy slowly spreads, $\Lambda(t)$ does not reach a constant positive value but rather decreases with a slope $\Lambda(t) \propto t^{-\nu}$, where $\nu < 1$. Similar behavior was also observed in Ref. [25] for a KG lattice, and this behavior was associated with nonequilibrium chaos.

To explain the initial oscillations of the mean energy position of m_2 and P, we show in Fig. 4(a) the power spectral density (PSD) of the velocity of particle $n = 56$, for a time window of length $\Delta t = 1.6\times10^3$ starting from $t = 0$. The largest peak of the PSD at frequency $\omega_1 \approx 3.189$ corresponds to the localized linear mode with frequency $\Omega_1 = 3.211$, also indicated by the (red) circle on the right of peak $\hat{F}_{\omega_1}$, which is shifted due to nonlinearity. The peaks at smaller frequencies correspond to other modes that were weakly excited from the beginning [see Fig. 1(d)]. A nonlinear shift to smaller frequencies appears for these peaks of the spectrum, too. The remaining peaks of the PSD correspond to second harmonics and all the linear combinations of the initial excited modes. By taking into account these nonlinear shifts, it appears that the two peaks at $\omega_2 \approx 2.176$ and $\omega_3 \approx 1.013$ are such that the condition $\omega_1 = \omega_2 + \omega_3$ is satisfied. It is exactly this resonance that allows the energy transfer from the dominant mode to the other two modes.

To monitor the time dependence of the different excited frequencies, we calculate the PSD of the velocity of particle $n = 56$ for a moving window Δt. In Fig. 4(b) we plot the evolution of the amplitude of the PSD at frequency ω_1, namely $\hat{F}_{\omega_1}$, and in Fig. 4(c) we show both the amplitudes $\hat{F}_{\omega_2}$ and $\hat{F}_{\omega_3}$ of the other frequencies (ω_2 and ω_3). We observe that the Fourier amplitudes perform characteristic oscillations, and whenever the amplitude of frequency ω_1 is decreasing, the amplitudes of ω_2 and ω_3 are increasing, and vice versa, indicating that energy is transferred between the three most excited nonlinear modes.

Furthermore, these oscillations have a direct impact on the evolution of $m_2(t)$ and $P(t)$ shown in Fig. 3, which can be explained as follows. The linear modes corresponding to the three interacting nonlinear modes are shown in Figs. 4(d)–4(f). The labeling of modes is done by ascending frequency order (i.e., mode 100 has the largest eigenfrequency). Mode $i = 98$, which is the dominant one, is very localized at particle $n = 56$, with a participation number $P \approx 2.7$. The other two modes ($i = 93,67$), however, are more extended (to the right of bead $n = 56$) with participation numbers $P \approx 5.98$ and $P \approx 8.25$ for $i = 93$ and 67, respectively. When energy is transferred from the dominant mode to the other two, the participation number P of the total energy distribution is expected to increase, along with m_2. This is exactly what we observe in Fig. 3.

B. Abrupt energy spreading

The evolution of the energy distribution, when the particle $n = 60$ is initially excited with energy $H = 0.192$, is shown in Fig. 2(b), and the wave packet appears to remain localized at least up to $t \approx 10^6$. As is shown in Fig. 5(a), during this time interval the energy spreading, as measured by m_2, is very slow since m_2 has a small positive slope. Then at $t \approx 2\times10^6$ an

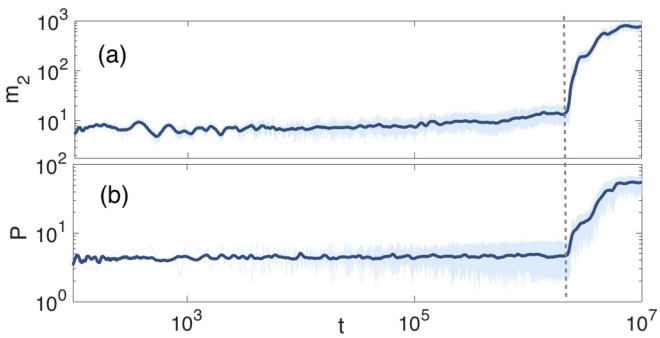

FIG. 5. Same as in Fig. 3, but for the initial excitation of particle $n = 60$ with energy $H = 0.192$.

abrupt spreading of energy appears as indicated by the vertical dashed line in Fig. 5 showing the sudden increase of m_2. A similar behavior is also found for the participation number P. It is found that initially [Fig. 5(b)] an average of five particles are involved in the dynamics of the chain, but after $t \approx 2\times10^6$ more degrees of freedom are excited and the participation number finally reaches a maximum value of $P \approx 60$ [this is the largest value of P obtained by the most extended linear modes shown in Fig. 1(c)]. Similar abrupt spreading has been previously observed in KG and DNLS systems [23].

The above description of the dynamics of the chain has a direct imprint in the evolution of the corresponding $\Lambda(t)$ shown in Fig. 2(j). There, we first observe a primal phase of regular behavior up to $t \approx 2\times10^4$. Then, during the very slow spreading phase, which follows for $2\times10^4 \lesssim t \lesssim 2\times10^6$, $\Lambda(t)$ starts deviating from the $\propto t^{-1}$ law taking a value $\Lambda(t) \approx 10^{-4}$. This behavior of $\Lambda(t)$ indicates that the weakly spreading phase is connected to a slow thermalization process induced by the corresponding chaotic dephasing of the initially excited normal modes. However, following the abrupt energy spreading discussed in the previous paragraph, $\Lambda(t)$ exhibits a "jump" to higher values. This jump is related to the transition of the motion from a "small chaotic sea," which is confined in a small subset of the system's phase space, i.e., the motion of a few sites around particle $n = 60$, to a "large chaotic sea," which occupies almost all phase space, i.e., the chaotic motion of the whole chain (a similar transition was reported in [34]).

C. Localized chaotic motion

In Fig. 2(c), we see the spatiotemporal evolution of the energy after exciting particle $n = 81$ with $H = 0.192$. Here we have a unique behavior. Contrary to the two other cases, we do not observe a destruction of the energy localization, at least for the considered integration times. The fact that energy remains localized is also seen by the running mean value of the second moment m_2 and the participation number P shown in Figs. 6(a) and 6(b), respectively, which are found to remain almost constant throughout the total time of integration. In fact, according to Fig. 2(c) only particles $n = 80-82$ significantly contribute in the dynamics of the system and thus $P \approx 2$.

What is more interesting in this case is that even though the energy remains confined, the system is found to be chaotic (nevertheless with a small Lyapunov exponent) with $\Lambda(t)$ reaching a constant value, as shown in Fig. 2(d). In addition,

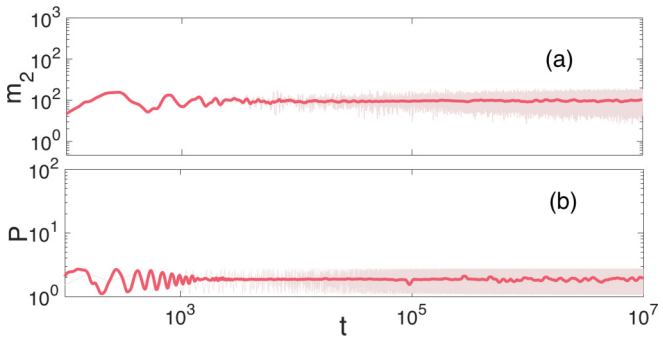

FIG. 6. Same as in Fig. 3, but for the initial excitation of particle $n = 81$ with energy $H = 0.192$.

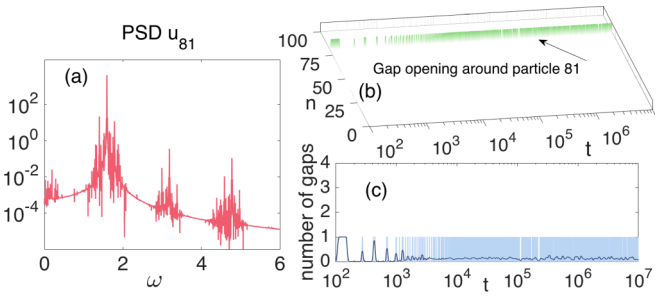

FIG. 7. (a) The PSD taken from the velocity of particle $n = 81$ for a time interval of duration $\Delta t = 5000$ time units, after $t = 4.95\times10^5$. (b) The gaps appearing in the chain as a function of time t and particle position n. (c) The total number of gaps in the chain as a function of time. The solid line indicates the running average.

the constancy of $\Lambda(t)$ for $t \gtrsim 2\times10^5$ stems from the fact that no more degrees of freedom are activated at least up to $t = 10^7$. Thus, for this particular case, chaoticity is not sufficient to induce the spreading of the wave packet. We note here that eventually this chaotic response could lead to energy spreading through very slow processes such as Arnold diffusion [35–37], but here a long-lasting spatially confined chaos is reported in a disordered, nondegenerate lattice system.

To further understand this behavior, we observe from the corresponding frequency spectrum shown in Fig. 7(a) that only a finite range of frequencies located around the fundamental ones (and their higher harmonics) are excited. However, the three particles that contribute to the evolution, i.e., $n = 80-82$, do not participate to linear modes within this range of frequencies [see the red square of Fig. 1(b)] and thus the energy remains confined to the particles $n = 80-82$. This qualitatively explains the robustness of this Anderson-like localization despite the chaotic nature of the wave packet.

We also note that, as shown in panels (b) and (c) of Fig. 7, during the evolution a single gap between particle $n = 81$ and its first neighbors appears. Note that no gap opening appears for the cases of particles $n = 56$ and 60. This observation is in line with the results of Ref. [38], where a localized chaotic behavior was found due to a nonsmooth nonlinearity. However, in that model the linear limit is described by uncoupled oscillators (one particle per mode), while in our case the localized Anderson-like excitation coexists with the extended modes.

IV. FATE OF LOCALIZATION: HIGHLY NONLINEAR REGIME

We furthermore study the dynamics of the chain after single-particle displacements with energies an order of magnitude larger than those of Fig. 2 to investigate the effect of stronger nonlinearities. Characteristic examples of the energy evolution in this regime are shown in Figs. 8(a) and 8(b), after the initial displacement of particles $n = 60$ and 81, respectively, with $H = 2.76$. Note that in both cases, in order to achieve such a large energy value, the initial displacement of the particles is larger than their overlap, δ_n, and initially a gap between beads is created. It is directly evident from Figs. 8(a) and 8(b) that both wave packets remain initially localized but finally spread throughout the whole chain, as is also indicated by

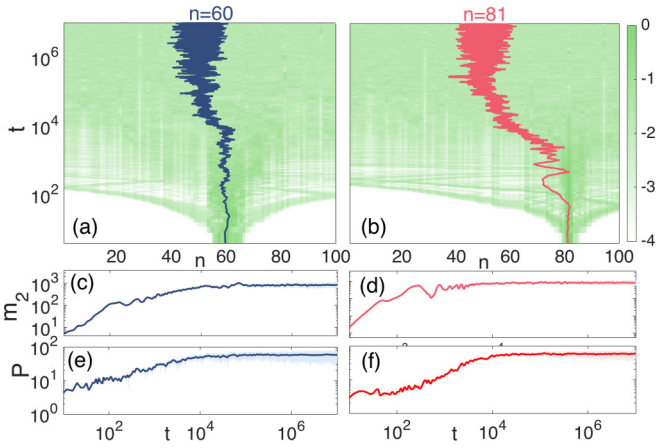

FIG. 8. (a) and (b) Contour plots showing the spatiotemporal evolution of the energy after exciting particles $n = 60$ (a) and $n = 81$ (b) with energy $H_1 = 2.76$. The color bar on the right is in logarithmic scale. (c) and (d) The second energy moment m_2 as a function of time for the corresponding top panels. (e) and (f) The participation number P corresponding to the evolution shown in panels (a) and (b), respectively. The solid lines in panels (c)–(f) indicate the running average.

the mean position of the energy distribution, which finally oscillates around the chain's center for $t \gtrsim 10^4$. The evolution of m_2 is quite similar for the two cases and is found to saturate around the same value $m_2 \approx 10^3$ [Figs. 8(c) and 8(d)]. Similarly, P saturates to a constant value around $P \approx 60$ for both excitations [Figs. 8(e) and 8(f)].

One of the most fundamental differences found between the dynamics for moderate and strong initial displacements is the evolution of gaps (contacts breaking) in the chain, shown in Fig. 9. For sufficiently strong initial excitations, according to the results shown in Figs. 9(a) and 9(b), the gap located around the originally excited particle induces additional gaps that are

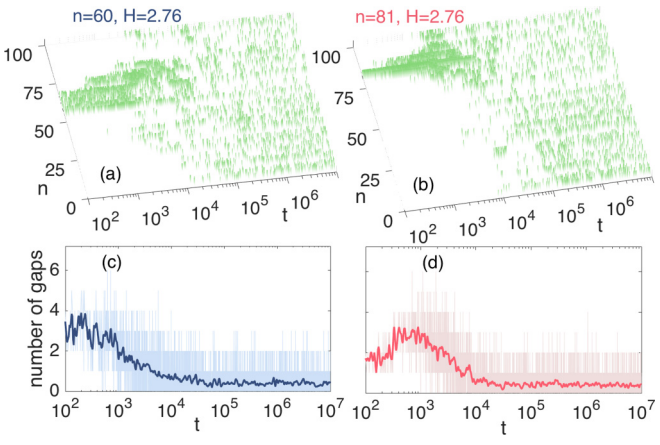

FIG. 9. (a),(b) The gaps appearing in the chain as a function of time t and particle position n for the case of initially exciting particle $n = 60$ (a) and particle $n = 81$ (b) with $H = 2.76$. Each gap is represented by a vertical segment. (c),(d) The total number of gaps in the chain as a function of time for the cases of panels (a) and (b), respectively. Solid lines correspond to the running average of each panel.

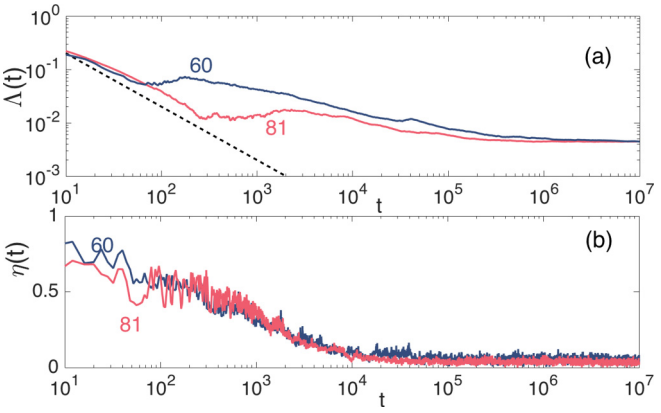

FIG. 10. (a) The finite-time mLCE $\Lambda(t)$ and (b) the spectral entropy $\eta(t)$ as a function of time for the cases of panels (a) and (b) of Fig. 8. The dashed line in (a) denotes the law $\Lambda(t) \propto t^{-1}$ appearing for the case of regular motion.

finally transmitted throughout the chain. In fact, according to the total number of gaps shown in Figs. 9(c) and 9(d), at different times more than one gap appears in the system. However, at the end of the simulations, for the two different excitations the running average of the number of gaps saturates to a value close to 1.

It is due to the above-mentioned differences that also the chaoticity in this regime, as quantified by $\Lambda(t)$ and shown in Fig. 10(a), is also different from the weakly nonlinear case. Here, a clear chaotic behavior for about four decades of our simulations ($10^2 \lesssim t \lesssim 10^6$) is found as $\Lambda(t)$ clearly deviates from the $\propto t^{-1}$ law [dashed line in Fig. 10(a)]. Furthermore, for both initial excitations, after about $t \approx 10^6$, $\Lambda(t)$ saturates to almost the same constant, positive value. The evolution of $\Lambda(t)$ for $10^2 \lesssim t \lesssim 10^6$ follows the transient chaotic behavior of the chain, where energy spreading takes place with more degrees of freedom being activated but also the number of gap openings is changing [see Figs. 9(a) and 9(b)].

The fact that the running average values of m_2, P (Fig. 8), the value of $\Lambda(t)$ (Fig. 10), and the number of gaps in the chain (Fig. 9) saturate to the same values for both excitations suggests that the system finally reaches an equilibrium state characterized by equipartition of energy. To quantify energy equipartition, we use the spectral entropy $S(t)$ defined by [39,40]

$$S(t) = -\sum_{k=1}^{N} w_k(t) \ln [w_k(t)], \tag{3}$$

where $w_k = E_k / \sum_{k=1}^{N} E_k$ are weights given by the fraction of the total harmonic energy E_k in the kth normal mode. We note that the value of E_k is obtained by projecting the displacement and momentum vectors $(\vec{u}(t), \dot{\vec{u}}(t))$ onto the linear normal modes $(\vec{Q}(t), \dot{\vec{Q}}(t))$ and calculating the energy associated with each mode $E_k = (\dot{Q}_k + \omega_k^2 Q_k)/2$. This entropy is equal to 0 if all the energy is associated with only one of the linear modes, say mode s, since then $w_s = 1$ and $w_{n \neq s} = 0$. On the other hand, S acquires its maximum value if energy equipartition is achieved and all modes carry the same amount of energy. Note that this maximum value depends on the total number

of oscillators N. To measure a quantity independent of the number of degrees of freedom, we calculate the normalized spectral entropy

$$\eta(t) = \frac{S(t) - S_{\max}}{S(t) - S(0)}, \tag{4}$$

where $S_{\max}$ is the maximum measured entropy. In this case, $\eta = 1$ indicates a "freezing" of the initial excitation, where all the energy remains in the initially excited modes, while $\eta \to 0$ denotes equipartition. From the evolution of $\eta(t)$ in Fig. 10(b), we observe that, after some relaxation time, $\eta(t)$ saturates to a value $\eta \approx 0.01$ for both initial excitations. This behavior strongly supports the assumption that a final equilibrium state, characterized by energy equipartition with the same statistical characteristics for any initial condition with the same total energy, is reached. Importantly, this is not always the case in the weakly nonlinear regime where only for particular initial excitations at a given energy is an equipartition reached [41]. This is the case of initially exciting particle $n = 60$ with $H = 0.192$ [shown in Fig. 2(b)], where we have confirmed an energy equipartition at the end of the simulation.

V. SUMMARY AND CONCLUSIONS

In this work, we studied the energy spreading and the chaotic behavior of a finite, nonlinear, and strongly disordered granular chain model. The considered system has two types of nonlinearities: smooth ones due to Hertzian contact interactions between neighboring particles, and nonsmooth nonlinearities related to contact breakings and the appearance of gaps in the chain.

An important outcome of our work is that based on the spatiotemporal properties of the corresponding linear lattice, we were able to propose a prescription for identifying initial single-particle excitations leading to localized energy propagation. As the system has both localized and extended eigenmodes, such initial single-particle displacements should be sought among the ones that do not excite low frequency, extended eigenmodes because such modes could, in principle, destroy localization. Aiming additionally at the generation of long-lived Anderson-like localization, one has to also further restrict the choice among these excitations by also considering the ones that excite as few as possible localized eigenmodes. This additional restriction decreases the possibility of the appearance of resonances between the excited modes, which in turn could lead to energy spreading. The visual identification of initial single-particle displacement excitations that satisfy these two conditions is facilitated by the creation of a contour plot of the size of the projection coefficients of all possible initial excitations onto the eigenmodes in the "eigenmode frequency"-"index of excited site" space [Fig. 1(b)]. We note that such plots could be used for finding also more general initial excitations that could lead to long-lasting energy localization.

Implementing this strategy, we managed to indeed identify several initial single-particle displacement excitations, which led to the creation of localized chaotic motions of various life spans. In Sec. III we discussed in detail the characteristics of three representative cases corresponding to the initial excitation of particles $n = 56$, 60, and 81 of the particular granular chain realization we considered here. The time evolution of the corresponding finite-time maximum Lyapunov exponent revealed the chaotic nature of all these cases. More specifically, we found an initial excitation ($n = 56$) that, after a transient localized phase, resulted in a rather slow energy spreading. This behavior was induced by the appearance of a nonlinear resonant interaction between the excited modes. In another case ($n = 60$), an initial phase of energy localization, characterized by an extremely slow spreading, was followed by an abrupt increase of chaoticity due to a jump in phase space from a "small" to a "large" chaotic sea, finally leading to extended chaotic motions and energy spreading throughout the lattice.

Another main outcome of our study was the presentation of an initial excitation ($n = 81$) that led to long-lived (at least until the final integration time of our simulations) energy localization. This is a significant result as we were able to provide an example of long-lasting, chaotic, Anderson-like localization in a system supporting extended eigenmodes. This initial excitation was identified by the above-mentioned prescription, and it led to the excitation of almost one eigenmode, which was practically isolated in the "frequency"-"site" space of Fig. 1(b), i.e., it did not have any strong interactions with other modes, and especially extended (low-frequency) modes were not sufficiently excited.

Finally, for sufficiently strong initial excitations the coexistence of anharmonic nearest-neighbor nonlinearities and gaps led to a chaotic destruction of localization, and the system finally reached an energy equipartition state, independent of the initial displacement excitation.

ACKNOWLEDGMENTS

G.T. acknowledges financial support from FP7-CIG (Project 618322 ComGranSol). Ch.S. acknowledges support by the National Research Foundation of South Africa (IFRR and CPRR Programmes) and thanks LAUM for its hospitality during his visits when part of this work was carried out.

[1] H. M. Jaeger and S. R. Nagel, Rev. Mod. Phys. **68**, 1259 (1996).

[2] J. K. Mitchell and K. Soga, *Fundamentals of Soil Behavior*, 3rd ed. (Wiley, New York, 2005); T. Aste and D. Weaire, *The Pursuit of Perfect Packing* (Institute of Physics, Bristol, 2000).

[3] B. Andreotti, Y. Forterre, and O. Pouliquen, *Granular Media: Between Fluid and Solid* (Cambridge University Press, New York, 2013).

[4] P. J. Yunker, K. Chen, M. D. Gratale, M. A. Lohr, T. Still, and A. G. Yodh, Rep. Prog. Phys. **77**, 056601 (2014).

[5] D. Kaya, N. L. Green, C. E. Maloney, and M. F. Islam, Science **329**, 656 (2010); K. Chen, W. G. Ellenbroek, Z. Zhang, D. T. N. Chen, P. J. Yunker, S. Henkes, C. Brito, O. Dauchot, W. van Saarloos, A. J. Liu, and A. G. Yodh, Phys. Rev. Lett. **105**, 025501 (2010); A. Ghosh, V. K. Chikkadi, P. Schall, J. Kurchan, and D. Bonn, *ibid.* **104**, 248305 (2010).

[6] K. Chen, T. Still, S. Schoenholz, K. B. Aptowicz, M. Schindler, A. C. Maggs, A. J. Liu, and A. G. Yodh, Phys. Rev. E **88**, 022315 (2013).

[7] E. T. Owens and K. E. Daniels, Soft Matter **9**, 1214 (2013).

[8] H. Hu, A. Strybulevych, J. H. Page, S. E. Skipetrov, and B. A. van Tiggelen, Nat. Phys. **4**, 945 (2008).

[9] L. A. Cobus, S. E. Skipetrov, A. Aubry, B. A. van Tiggelen, A. Derode, and J. H. Page, Phys. Rev. Lett. **116**, 193901 (2016).

[10] S. Sen, J. Hong, J. Bang, E. Avalos, and R. Doney, Phys. Rep. **462**, 21 (2008).

[11] G. Theocharis, N. Boechler, and C. Daraio, in *Acoustic Metamaterials and Phononic Crystals* (Springer, New York, 2013), pp. 217–251.

[12] L. Ponson, N. Boechler, Y. M. Lai, M. A. Porter, P. G. Kevrekidis, and C. Daraio, Phys. Rev. E **82**, 021301 (2010).

[13] B. P. Lawney and S. Luding, Acta Mech. **225**, 2385 (2014).

[14] C. Chong, M. A. Porter, P. G. Kevrekidis, and C. Daraio, J. Phys.: Condens. Matter **29**, 413003 (2017).

[15] M. Manciu, S. Sen, and A. Hurd, Physica D **157**, 226 (2001).

[16] M. Manjunath, A. P. Awasthi, and P. H. Geubelle, Phys. Rev. E **85**, 031308 (2012).

[17] M. Przedborski, S. Sen, and T. A. Harroun, J. Stat. Mech. (2017) 123204.

[18] A. J. Martínez, P. G. Kevrekidis, and M. A. Porter, Phys. Rev. E **93**, 022902 (2016).

[19] V. Achilleos, G. Theocharis, and Ch. Skokos, Phys. Rev. E **93**, 022903 (2016).

[20] R. K. Shrivastava and S. Luding, Nonlin. Proc. Geophys. **24**, 435 (2017).

[21] G. Kopidakis, S. Komineas, S. Flach, and S. Aubry, Phys. Rev. Lett. **100**, 084103 (2008); A. S. Pikovsky and D. L. Shepelyansky, *ibid.* **100**, 094101 (2008); S. Flach, D. O. Krimer, and Ch. Skokos, *ibid.* **102**, 024101 (2009); I. García-Mata and D. L. Shepelyansky, Phys. Rev. E **79**, 026205 (2009); T. V. Laptyeva, J. D. Bodyfelt, D. O. Krimer, Ch. Skokos, and S. Flach, Europhys. Lett. **91**, 30001 (2010); Ch. Skokos and S. Flach, Phys. Rev. E **82**, 016208 (2010); S. Flach, Chem. Phys. **375**, 548 (2010); J. D. Bodyfelt, T. V. Laptyeva, Ch. Skokos, D. O. Krimer, and S. Flach, Phys. Rev. E **84**, 016205 (2011); Ch. Antonopoulos, T. Bountis, Ch. Skokos, and L. Drossos, Chaos **24**, 024405 (2014).

[22] H. Veksler, Y. Krivolapov, and S. Fishman, Phys. Rev. E **80**, 037201 (2009); D. Basko, Ann. Phys. (NY) **326**, 1577 (2011); J. D. Bodyfelt, T. V. Laptyeva, G. Gligoric, D. O. Krimer, Ch. Skokos, and S. Flach, Int. J. Bifurcation Chaos **21**, 2107 (2011); M. Mulansky and A. Pikovsky, Phys. Rev. E **86**, 056214 (2012); T. V. Laptyeva, J. D. Bodyfelt, and S. Flach, Europhys. Lett. **98**, 60002 (2012); M. Mulansky and A. Pikovsky, New J. Phys. **15**, 053015 (2013); M. V. Ivanchenko, T. V. Laptyeva, and S. Flach, Phys. Rev. B **89**, 060301(R) (2014); T. V. Laptyeva, M. V. Ivanchenko, and S. Flach, J. Phys. A **47**, 493001 (2014).

[23] Ch. Skokos, D. O. Krimer, S. Komineas, and S. Flach, Phys. Rev. E **79**, 056211 (2009).

[24] O. Tieleman, Ch. Skokos, and A. Lazarides, Europhys. Lett. **105**, 20001 (2014).

[25] Ch. Skokos, I. Gkolias, and S. Flach, Phys. Rev. Lett. **111**, 064101 (2013).

[26] M. V. Ivanchenko, T. V. Laptyeva, and S. Flach, Phys. Rev. Lett. **107**, 240602 (2011).

[27] K. L. Johnson, *Contact Mechanics* (Cambridge University Press, Cambridge, 1985); V. F. Nesterenko, *Dynamics of Heterogeneous Materials* (Springer, New York, 2001).

[28] J. Fabian, Phys. Rev. B **55**, R3328(R) (1997); D. M. Leitner, *ibid.* **64**, 094201 (2001).

[29] P. K. Datta and K. Kundu, Phys. Rev. B **51**, 6287 (1995).

[30] É. Forest and R. D. Ruth, Physica D **43**, 105 (1990); H. Yoshida, Phys. Lett. A **150**, 262 (1990).

[31] G. Benettin, L. Galgani, A. Giorgilli, and J.-M. Strelcyn, Meccanica **15**, 9 (1980); **15**, 21 (1980).

[32] Ch. Skokos, Lect. Notes Phys. **790**, 63 (2010).

[33] Ch. Skokos and E. Gerlach, Phys. Rev. E **82**, 036704 (2010); E. Gerlach and Ch. Skokos, Discrete Cont. Dyn. Sys.-Supp. 475 (2011); E. Gerlach, S. Eggl, and Ch. Skokos, Int. J. Bifurcation Chaos **22**, 1250216 (2012).

[34] G. Contopoulos, L. Galgani, and A. Giorgilli, Phys. Rev. A **18**, 1183 (1978).

[35] V. I. Arnold, Sov. Math. Dokl. **5**, 581 (1964).

[36] A. J. Liechtenberg and M. Lieberman, *Regular and Chaotic Dynamics* (Springer-Verlag, Berlin, 1992).

[37] Arnold diffusion in systems with more than 2 degrees of freedom can allow chaotic motion to propagate to phase-space regions far away from the motion's origin through a web of (possibly infinitesimally thin) interconnected chaotic layers.

[38] S. Roy and A. Pikovsky, Chaos **22**, 026118 (2012).

[39] R. Livi, M. Pettini, S. Ruffo, M. Sparpaglione, and A. Vulpiani, Phys. Rev. A **31**, 1039 (1985).

[40] L. Casetti, M. Cerruti-Sola, M. Pettini, and E. G. D. Cohen, Phys. Rev. E **55**, 6566 (1997).

[41] M. Mulansky, K. Ahnert, A. Pikovsky, and D. L. Shepelyansky, Phys. Rev. E **80**, 056212 (2009).